Since January 2020 Elsevier has created a COVID-19 resource centre with free information in English and Mandarin on the novel coronavirus COVID-19. The COVID-19 resource centre is hosted on Elsevier Connect, the company's public news and information website.

International Immunopharmacology 103 (2022) 108463

Contents lists available at ScienceDirect

International Immunopharmacology

journal homepage: www.elsevier.com/locate/intimp

The JAK inhibitor ruxolitinib abrogates immune hepatitis instigated by concanavalin A in mice

Mohamed E. Shaker [a,b,*], Omnia M. Hendawy [a,c], Mohamed El-Mesery [d], Sara H. Hazem [b]

[a] Department of Pharmacology, College of Pharmacy, Jouf University, Sakaka 72341, Aljouf, Saudi Arabia
[b] Department of Pharmacology and Toxicology, Faculty of Pharmacy, Mansoura University, Mansoura 35516, Egypt
[c] Department of Clinical Pharmacology, Faculty of Medicine, Beni-Suef University, Beni-Suef, Egypt
[d] Department of Biochemistry, Faculty of Pharmacy, Mansoura University, Mansoura 35516, Egypt

ARTICLE INFO

Keywords:
Concanavalin A
Ruxolitinib
JAK
Immune Hepatitis
Cytokine Storm

ABSTRACT

Therapeutics that impair the innate immune responses of the liver during the inflammatory cytokine storm like that occurring in COVID-19 are greatly needed. Much interest is currently directed toward Janus kinase (JAK) inhibitors as potential candidates to mitigate this life-threatening complication. Accordingly, this study investigated the influence of the novel JAK inhibitor ruxolitinib (RXB) on concanavalin A (Con A)-induced hepatitis and systemic hyperinflammation in mice to simulate the context occurring in COVID-19 patients. Mice were orally treated with RXB (75 and 150 mg/kg) 2 h prior to the intravenous administration of Con A (20 mg/kg) for a period of 12 h. The results showed that RXB pretreatments were efficient in abrogating Con A-instigated hepatocellular injury (ALT, AST, LDH), necrosis (histopathology), apoptosis (cleaved caspase-3) and nuclear proliferation due to damage (PCNA). The protective mechanism of RXB were attributed to i) prevention of Con A-enhanced hepatic production and systemic release of the proinflammatory cytokines TNF-α, IFN-γ and IL-17A, which coincided with decreasing infiltration of immune cells (monocytes, neutrophils), ii) reducing Con A-induced hepatic overexpression of IL-1β and CD98 alongside NF-κB activation, and iii) lessening Con A-induced consumption of GSH and GSH peroxidase and generation of oxidative stress products (MDA, 4-HNE, NOx) in the liver. In summary, JAK inhibition by RXB led to eminent protection of the liver against Con A-deleterious manifestations primarily *via* curbing the inflammatory cytokine storm driven by TNF-α, IFN-γ and IL-17A.

1. Introduction

Nowadays, the interplay that occurs between different signaling pathways of proinflammatory cytokines in the setting of acute inflammation has gained much interest due to the evolution of the COVID-19 pandemic [1,2]. Much effort is currently exerted toward identifying therapeutic approaches for targeting multiple pathways to limit the COVID-19-elicited inflammatory cytokine storm that damages not only the lungs, but also other organs like the liver [3,4]. The Janus kinase-signal transducer and activator of transcription (JAK-STAT) cascade is one of these pathways that is currently under scientific focus. The JAK-STAT pathway is essential for hematopoiesis and immune cell development, because of its key role in transducing cell signals arising from the membrane-receptors to the nucleus [1]. JAKs are currently believed to orchestrate the inflammatory downstream and upstream signaling of myriad cytokines and growth factors like IL-6, IFN-γ, TNF-α, IL-1β, IL-22 and others [5]. In the liver, JAKs 1 and 2 have shown to be implicated in different contexts of liver injury like ischemia/reperfusion [6], carcinogenesis [7] and fibrosis [8].

In the last decade, JAK inhibitors (jakinibs) have emerged as a remarkable pharmacological class for cancer and autoimmune inflammatory disorders [9,10]. Ruxolitinib (RXB) is an oral jakinib that was originally FDA-approved for myelofibrosis, followed by approval in polycythemia vera and recently, graft versus host disease [11–13]. Currently, RXB is under investigations in COVID-19 patients with hyperinflammation [14–16]. Pharmacologically, RXB is a small molecule that blocks the ATP-binding catalytic region of the kinase domain for JAKs 1 and 2 at nanomolar concentrations [12].

The lectin concanavalin A (Con A) is a strong T cell mitogen that selectively damages the liver. The Con A-mouse model is supposed to be driven by massive cytokine release from activated T cells, Kupffer cells and infiltrated immune cells, leading to hepatic injury characterized by

* Corresponding author.
E-mail addresses: melsayed@ju.edu.sa, mshaker2222@yahoo.com (M.E. Shaker).

https://doi.org/10.1016/j.intimp.2021.108463
Received 17 September 2021; Received in revised form 1 December 2021; Accepted 12 December 2021
Available online 21 December 2021

necrotic and apoptotic cell death [17]. Because this model has a strong similarity to immune-provoked inflammation in humans' livers like that occurring in autoimmune hepatitis and acute viral hepatitis [18], it is ideal for investigating emerging therapies that affect the innate immune responses of the liver during the inflammatory cytokine storm. Accordingly, the current study aimed to examine the impact of JAK inhibition by the small molecule RXB on Con A-induced hepatitis.

2. Materials and methods

2.1. Mice

Male BALB/c mice (28 ± 2 g) were housed in cages supplied with water and regular chow throughout the study period. The animal caring, monitoring and procedures were following the criteria of the NIH and the regulations of the Research Ethics Committee for Care of Laboratory Animals approved by the institutions.

2.2. RXB treatment and Con A model of acute liver injury

RXB powder (as a phosphate salt, Novartis, Switzerland) was suspended as 0.75 and 1.5% w/v in a solution of sterile saline composed of 0.5% w/v of carboxymethylcellulose. Con A powder (Sigma-Aldrich, USA) was dissolved as 0.2% w/v in a sterile water for injection. The first group of mice received the vehicle devoid of RXB (oral) and sterile water (IV injection in tail vein) after 2 h and acted as the normal control group. The second group of mice received the vehicle devoid of RXB (oral) and Con A (20 mg/kg) in sterile water (IV) 2 h afterwards. The last 2 groups of mice received RXB doses (75 or 150 mg/kg, oral) in their vehicle and Con A (20 mg/kg, IV) in sterile water (IV) 2 h afterwards. After 12 h from Con A administration, the mice were administered thiopental (100 mg/kg, intraperitoneal) for anesthesia. Blood samples were taken from the heart after ventral incision and left to clot for 20 min prior to centrifugation at 5000 g for 10 min at 25 °C for serum separation and storage −80 °C. Liver tissue samples were washed with saline and transferred to an ultra-freezer for keeping them at −80 °C for cytokine and oxidative stress assessments. Pieces of liver were also transferred to a solution of 4% (v/v) neutral-buffered formalin for histopathological and immunohistochemical evaluations.

2.3. Biochemical evaluation of hepatic injury

Aminotransferase (ALT), aspartate aminotransferase (AST) and lactate dehydrogenase (LDH) activities were quantified in mice blood sera to assess the severity of liver injury by commercial kits (Spectrum-diagnostics, Egypt).

2.4. Histopathological evaluation of hepatic injury

Paraffin blocks were prepared from fixed liver pieces, followed by installing on a microtome and cutting sections of 5 μm thickness. Thereafter, sections were mounted on glass slides and subjected to the staining protocol of hematoxylin and eosin. The intensity of hepatic necroinflammation was evaluated according to the assigned scores (0 = absent; 1 = mild; 2 = moderate; 3 = severe) by a pathologist blind to the experimental groups.

2.5. Immunostichemical evaluation of hepatic expression of NF-κB, cleaved caspase 3 , PCNA, F4/80 and CD98

Liver sections were cut similarly by the microtome and transferred to coated glass slides. Then, the conventional procedures of immunohistochemistry were followed for restoring antigenicity, neutralizing sample peroxidases and blocking the unspecific protein binding. Liver sections were incubated with primary antibodies for nuclear factor-kappa B (NF-κB) (BioLegend, USA), cleaved caspase 3 (Santa Cruz, USA), F4/80 (BioLegend, USA), proliferating cell nuclear antigen (PCNA) (BioLegend, USA) or CD98 (Santa Cruz, USA). After washing, liver sections bound to the primary antibodies were incubated with the optimal secondary antibodies, followed by the substrate and chromogen for visualization of the antigen. The percentage of expression or count of positive nuclei per field was determined through analyzing representative pictures by the ImageJ software (NIH, USA).

2.6. ELISA of hepatic and serum cytokines

Tumor necrosis factor-α (TNF-α), interferon-γ (IFN-γ), and interleukins (ILs)-17A, 10 and 1β were determined in both the liver lysates and sera. Liver lysates were prepared by homogenizing the liver (10% w/v) in the cold lysis buffer (150 mM NaCl, 0.5% v/v Triton X-100, 10 mM Tris pH 7.4, protease inhibitor mixture). Then, the mixture tubes were centrifuged at 6000 *g* for 10 min at 4 °C for isolating supernatants. The specimens of liver lysates and sera were added to wells of ELISA plates that were coated with a specific capture antibody the night before. The assay was finally completed by following the instructions supplied with the kits (BioLegend, USA). The protein concentration was also quantified in the liver lysates according to the previously described method [19].

2.7. Hepatic antioxidant enzymes and lipid peroxidation

Portions of liver tissue (10% w/v) were homogenized by a glass grinder in a freshly prepared buffer (20 mM Tris-HCl, 1 mM EDTA, pH 7.4), followed by centrifuging the homogenate at 3000 g for 20 min at 4 °C and isolation of supernatants from the settled pellets. The protein concentration was then determined spectrophotometrically by commercial kits (Spectrum-diagnostics, Egypt).

2.7.1. Hepatic superoxide dismutase (SOD) determination

Superoxide dismutase (SOD) activity was determined in the liver based on the method of inhibiting pyrogallol autoxidation [20]. In brief, liver homogenate samples were prepared as previously described [21], followed by mixing 0.07 ml of sample with 1 ml of 20 mM Tris-HCl (containing 1 mM EDTA, pH 8.5) and 0.07 ml of 15 mM pyrogallol (Alpha-Chem, India). Then, the elevation in absorbances over 3 min was monitored for the samples and a control with a buffer without sample at 420 nm. The percentage of inhibition for the samples was calculated and SOD activity was estimated as U/mg protein (1 unit is equivalent to the amount that inhibits the autoxidation rate of pyrogallol by 50%).

2.7.2. Hepatic reduced glutathione (GSH) determination

The concentration of reduced glutathione (GSH) was determined as previously described [22]. First, 25 μL of 50% (w/v) trichloroacetic acid was added to 225 μL of liver homogenate samples, followed by centrifugation at 3000 *g* for 10 min at 4 °C. Finally, 125 μL of the supernatants were diluted in 1000 μL of assay buffer (0.2 M Tris-HCl, 1 mM EDTA, pH 8.9) and 50 μL of 10 mM 5,5′-dithiobis (2-nitrobenzoic acid) (Sigma-Aldrich, USA) in methanol. The yellow color formed was measured spectrophotometrically at a wavelength of 412 nm, and samples concentrations were calculated from a standard curve of GSH concentration (Acros Organics, USA).

2.7.3. Hepatic GSH transferase determination

The activity of GSH transferase was estimated as previously described [23]. Ten microliter of 100 mM GSH in water and 10 μL of ethanol containing 100 mM 1-chloro-2,4-dinitrobenzene were premixed with 975 μL of the reaction buffer (0.8% w/v NaCl, 0.02% w/v KCl, 0.144% w/v Na_2HPO_4, 0.024% w/v KH_2PO_4, pH 6.5). Then, 5 μL of liver homogenate or buffer was added to the reaction mixture and the rise in absorbance at 340 nm was recorded after 1 min. GSH transferase activity was expressed as U/mg protein (1 unit of the enzyme is equivalent to the amount that conjugates 1 μM 1-chloro-2,4-dinitrobenzene and GSH in 1

min at 25 °C).

2.7.4. Hepatic GSH peroxidase determination

The activity of GSH peroxidase was estimated as previously described [25] with minor differences. First, 100 μL of 10 mM GSSG, 10 μL of GSH reductase (10 U/ml), 100 μL of 1 mM NADPH (dissolved in 50 mM NaH_2PO_4, 0.4 mM EDTA, pH 7) and 100 μL of liver homogenate (or the homogenization buffer) were added to 640 μL of the reaction buffer (50 mM NaH_2PO_4, 0.4 mM EDTA, 1 mM sodium azide, pH 7). Following incubation for 5 min, the decrease in absorbance after 1 min was recorded at 340 nm after adding 50 μL of 5 mM H_2O_2. GSH peroxidase activity was expressed as mU/mg protein (1 unit is equivalent to the concentration that causes the oxidation of 1 μM NADPH to $NADP^+$ over 1 min at 25 °C).

2.7.5. Hepatic GSH reductase determination

The activity of GSH reductase was assessed in the liver based on the previous assay [26]. Hundred microliter of 10 mM GSSG in water was added to 700 μL of the reaction buffer (50 mM NaH_2PO_4, 0.4 mM EDTA, 1 mM sodium azide, pH 7). After 5 min of incubation, 100 μL of 1 mM NADPH (freshly prepared in 50 mM NaH_2PO_4, 0.4 mM EDTA, pH 7) and 100 μL of liver homogenate (or the homogenization buffer) were added to the reaction buffer. Then, the decline in absorbance for samples and blank over 1 min was recorded at 340 nm. GSH reductase activity was expressed as mU/mg protein (1 unit of the enzyme is equivalent to the amount that cause the oxidizes 1 μM NADPH to $NADP^+$ over 1 min at 25 °C).

2.7.6. Hepatic malondialdehyde (MDA) and 4-hydroxynonenal (4-HNE) determinations

Colorimetric analysis was used to determine the hepatic malondialdehyde (MDA) and 4-hydroxynonenal (4-HNE) concentrations as previously mentioned [24]. First, 0.4 ml of aliquot from liver homogenate was added to 0.66 ml of the chromogen reagent [0.495 ml of 10.3 mM 1-methyl-2-phenylindole (Sigma, USA) freshly mixed with 0.165 ml of 32 μM $FeCl_3$ in methanol] in Eppendorf tubes. Second, 0.15 ml of concentrated HCl or methanesulfonic acid (Merck, Germany) was added to the tubes for determination of MDA only or MDA alongside 4-HNE, respectively. Then, the tubes were closed and were heated at 45 °C for a period of 60 min and 40 min. At the end, the tubes were cooled and centrifuged at 4000 *g* for 10 min. The absorbances of the clear samples were determined against sample blanks in a spectrophotometer at a wavelength of 586 nm. Incremental concentrations of tetramethoxypropane (Sigma, USA) or 4-HNE (Cayman, USA) were used for construction of the standard calibration curves. The concentration of 4-HNE only was obtained by subtracting the concentration of MDA from that of MDA alongside 4-HNE.

2.7.7. Hepatic total nitrate/nitrite (NOx) determination

The total nitrate/nitrite (NOx) was quantified in the liver as previously described [25]. In brief, 50 μL of 25% (w/v) sulfosalicylic acid was added to 450 μL of liver homogenate samples or the blank. After 10 min, the tubes were centrifuged at 3000 *g* for 15 min at 4 °C to isolate the precipitated sample proteins. Then, 300 μL of sample supernatants were added to Eppendorf tubes containing 300 μL 0.8% (w/v) vanadium trichloride (Acros Organics, USA) in 1 M HCl and 400 μL of a mixture (1:1) composed of 2% (w/v) sulfanilamide in 5% (v/v) HCl and 0.1% (w/v) N-(1-naphthyl) ethylendiamine dihydrochloride. The tubes were then kept at 37 °C for 45 min until a violet color produced that its absorbance was quantified spectrophotometrically at 540 nm. A standard curve of incremental concentrations of sodium nitrate was also analyzed under the same assay conditions for quantification of NOx in the samples.

2.7.8. Hepatic myeloperoxidase (MPO) determination

Myeloperoxidase (MPO) enzyme activity of the liver was determined spectrophotometrically at a wavelength of 650 nm as previously mentioned [26]. After centrifugation of the liver homogenate and isolation of supernatants, 50 mg of the settled pellet was transferred to clean Eppendorf tubes, washed with 1000 μL of the buffer (20 mM NaH2PO4, 100 mM NaCl, 15 mM EDTA, pH 4.7) and centrifuged at 5500g for 15 min at 4 °C. After discarding the supernatants, 500 μL 0.5% (w/v) of hexadecyltrimethylammonium bromide (MP Biomedicals, USA) in 50 mM sodium phosphate buffer (pH 5.4) was added to the tubes. Thereafter, the tubes were subjected to repeated freezing and thawing 3 times, followed by heating at 60 °C for 2 h and final centrifugation at 5500 g for 15 min at 4 °C. Two hundred microliter of the samples was added to 800 μL of the reaction buffer (50 mM sodium-phosphate buffer pH 5.4, 2 mM hydrogen peroxide), followed by adding 200 μL of 1.6 mM tetramethylbenzidine (MP Biomedicals, USA) in DMSO. MPO activity was determined by monitoring the increase in absorbance over 5 min, followed by determining the change equivalent to g of tissue.

2.8. Statistical analysis

All experimental data were expressed as means ± SE. All data, except the those of necroinflammation scores, were parametric and their statistical significances were calculated by one way ANOVA, followed by the post test of Tukey-Kramer. Meanwhile, the non-parametric Kruskal-Wallis test, ensued by the post test of Dunn's multiple comparison, was used for determining the statistical significance of the necroinflammation scores. The GraphPad Prism 8 (USA) was the used software in the statistical analysis of all data.

3. Results

3.1. RXB abrogates Con A-induced injury and necroinflammation of the liver

IV administration of Con A to mice caused a significant ($P < 0.001$) rise of serum ALT, AST and LDH activities in comparison the normal control counterparts (Fig. 1A-C). The histological evaluation and quantification of the Con A-liver sections showed pronounced ($P < 0.001$) elevation of hepatic necrosis and inflammation scores, while the normal mice were having normal liver architecture with the absence of hepatic necrosis and inflammation (Fig. 1D, E). Interestingly, RXB pretreatments (75 and 150 mg/kg) markedly abrogated Con A-provoked alterations of these biochemical and histopathological assessments in a dose-dependent manner.

3.2. RXB hinders the inflammation cascade driven by Con A in the liver

To ascertain whether the beneficial effect of RXB on Con A-hepatic injury was related to hindering the inflammation cascade, we assessed the changes in the proinflammatory cytokines TNF-α, IFN-γ and IL-17A alongside the anti-inflammatory cytokine IL-10. In comparison to the control mice, challenging mice by Con A led to significant rises of TNF-α, IFN-γ, IL-17A and IL-10 concentrations in both the serum and liver samples (Fig. 2). However, RXB treatments prior to exposure to Con A-challenge efficiently suppressed these significant rises of cytokines, especially at the dose level of 150 mg/kg.

3.3. RXB alleviates Con A-induced activation of NF-κB and overexpression of IL-1β in the liver

The crosstalk between proinflammatory cytokines is known to occur in the setting of hepatitis. Next, we assessed the changes of RXB pretreatments on the immunohistochemical expression of NF-κB and concentration of IL-1β in the mice livers challenged by Con A. The data indicated that cytoplasmic expression and nuclear translocation of NF-κB in the hepatic cells was increased by Con A, but this increase was

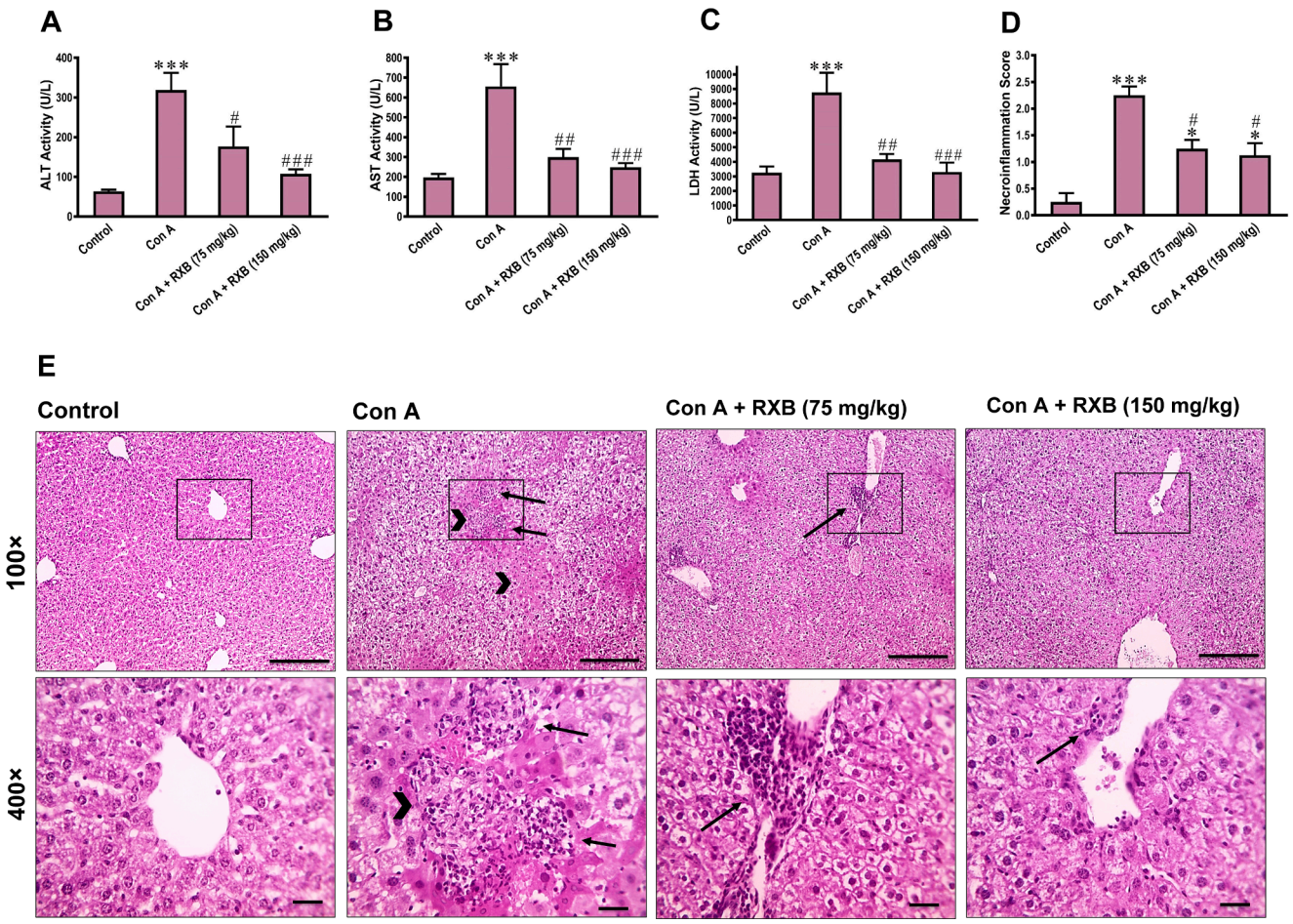

Fig. 1. Impact of RXB pretreatments (75 and 150 mg/kg) for Con A-challenged mice on serum ALT (A), AST (B) and LDH (C) activities, as well as the necroinflammation score (D) and histopathology (E; 100 and 400×; scale bars = 100 and 50 μm) of the liver (n = 6–8/group). Arrows indicate inflammatory infiltrates and arrowheads indicate necrotic areas. * and *** denote a P-value (vs. the Control) less than 0.05 and 0.001, respectively, but #, ## and ### denote a P-value (vs. the Con A) less than 0.05, 0.01 and 0.001, respectively.

minimal by RXB pretreatments (Fig. 3 A, B). Similarly, Con A induced overexpression of IL-1β in the mice livers, which was significantly inhibited by both doses of RXB (Fig. 3C). Of note, serum IL-1β concentration was not elevated in mice administered Con A alone or with RXB pretreatments (Fig. 3D).

3.4. RXB limits Con A-induced apoptosis and neutrophil infiltration in the liver

We next examined whether RXB can mitigate Con A-induced apoptosis by evaluating cleaved caspase 3 immunostaining in liver sections. While Con A led to a marked ($P < 0.001$ vs normal) increase in the number of hepatocytes positive for cleaved caspase 3, RXB pretreatments abated this increase of cleaved caspase 3, especially the dose of 150 mg/kg (Fig. 4A, C). Next, the impact of RXB pretreatments on Con A-induced changes in infiltration of immune cells in the liver was investigated by evaluating F4/80 immunohistochemical expression and MPO activity. In comparison to normal mice, Con A-administration to mice led to significant increase of F4/80 positive cells ($P < 0.01$ vs. control) in liver sections (Fig. 4B, D) and hepatic MPO activity ($P < 0.001$ vs. control) (Fig. 4 E). Noteworthy, Con A-induced elevation in both indices for infiltrating immune cells was efficiently prevented by 150 mg/kg of RXB pretreatment only.

3.5. RXB inhibits Con A-induced rise of nuclear PCNA in the liver

Hepatocellular injury drives nuclear repair for affected hepatocytes in order to recover the liver. Thereby, we assessed the changes of nuclear PCNA in hepatocytes of Con A-mice received no or RXB pretreatment by immunohistochemistry. The data indicated that the number of PCNA positive hepatocytes per field was increased in Con A-mice received no treatment (Fig. 5A, C). Meanwhile, pretreating the Con A-mice with RXB caused a marked decrease in the increased number of PCNA positive hepatocytes elicited by Con A alone.

3.6. RXB abates Con A-induced elevation of CD98 in the liver

Overexpression of CD98 has recently emerged as a driver for inflammation in immune and epithelial cells. Next, we investigated whether the ameliorative impact of RXB on Con A-hepatic insult is mediated by countering CD98 as well. In comparison to the normal group, Con A-administration led to overexpression of the hepatic CD98 in the mice (Fig. 5B, D). However, pretreating the mice with RXB (75 and 150 mg/kg) prior Con A significantly abated the expression of hepatic CD98.

3.7. RXB reverses Con A-induced abnormalities in GSH and its related enzymes in the liver

The contribution of the non-enzymatic antioxidant GSH and its

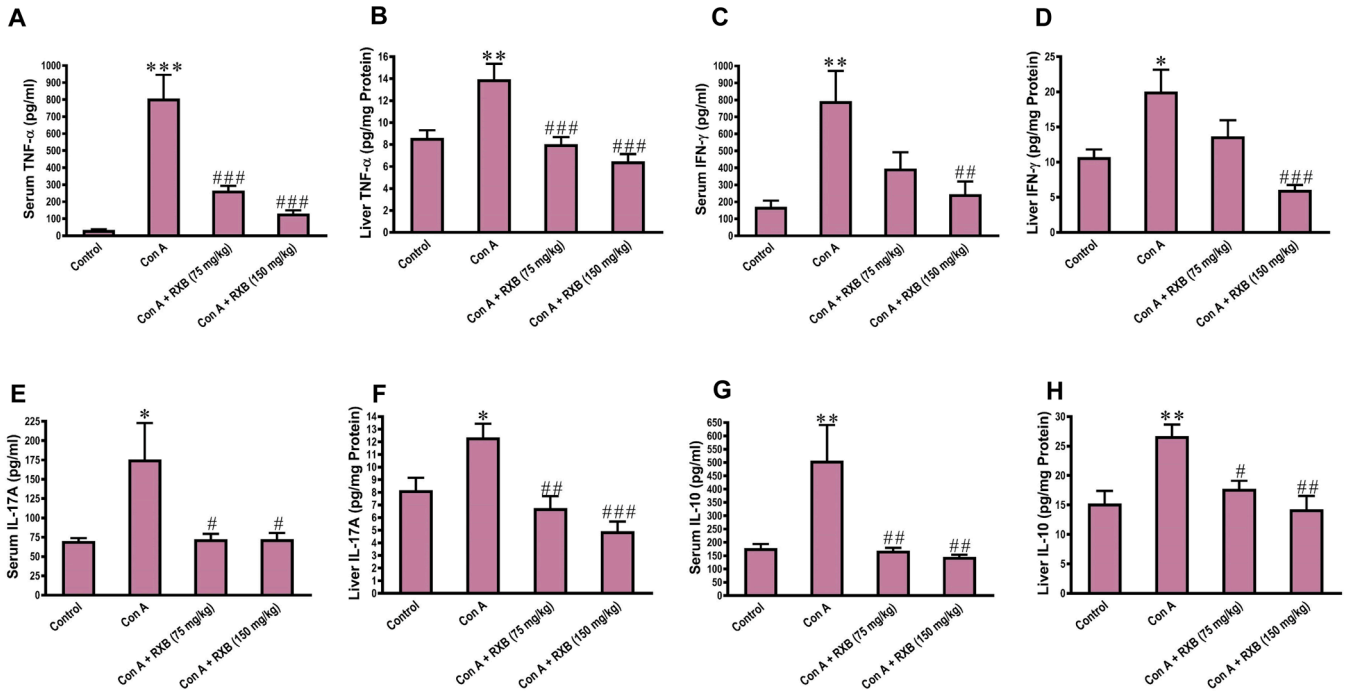

Fig. 2. Impact of RXB pretreatments (75 and 150 mg/kg) for Con A-challenged mice on the serum and hepatic concentrations of TNF-α (A, B), IFN-γ (C, D), IL-17A (E, F) and IL-10 (G, H) (n = 6–8/group). *, ** and *** denote a P-value (vs. the Control) less than 0.05, 0.01 and 0.001, respectively, but #, ## and ### denote a P-value (vs. the Con A) less than 0.05, 0.01 and 0.001, respectively.

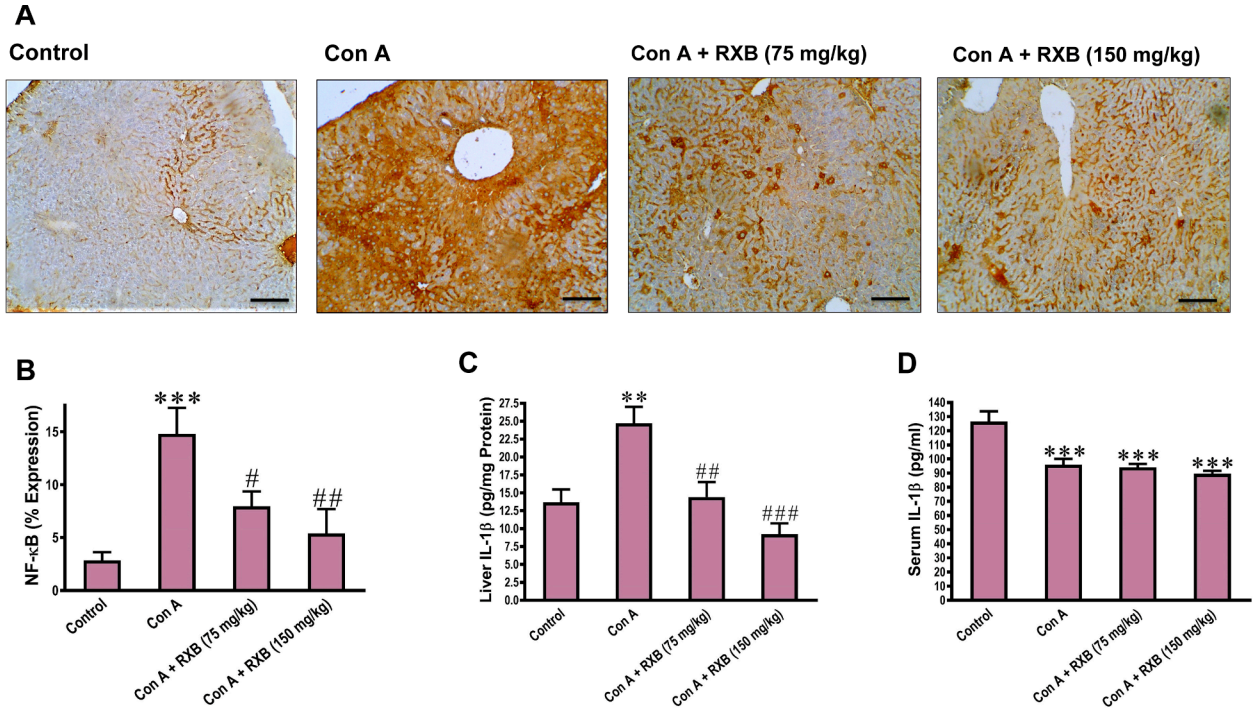

Fig. 3. Impact of RXB pretreatments (75 and 150 mg/kg) for Con A-challenged mice on the hepatic immunohistochemical expression and quantification of NF-κB (A and B; 100×; scale bar = 100 μm) and hepatic and serum concentrations of IL-1β (C and D) (n = 6–8/group). ** and *** denote a P-value (vs. the Control) less than 0.01 and 0.001, respectively, but #, ## and ### denote a P-value (vs. the Con A) less than 0.05, 0.01 and 0.001, respectively.

related enzymes including GSH peroxidase, GSH reductase and GSH transferase has yet to be unraveled in the context of immune hepatitis driven by Con A. In comparison to the normal mice, administering Con A to mice significantly reduced GSH ($P < 0.001$) and GSH peroxidase ($P < 0.05$), but unexpectedly raised GSH reductase ($P < 0.01$) and GSH transferase ($P < 0.001$) (Fig. 6A-D). Intriguingly, RXB treatments before exposure to Con A reversed these abnormalities in GSH and its related enzymes in the liver caused by Con A alone.

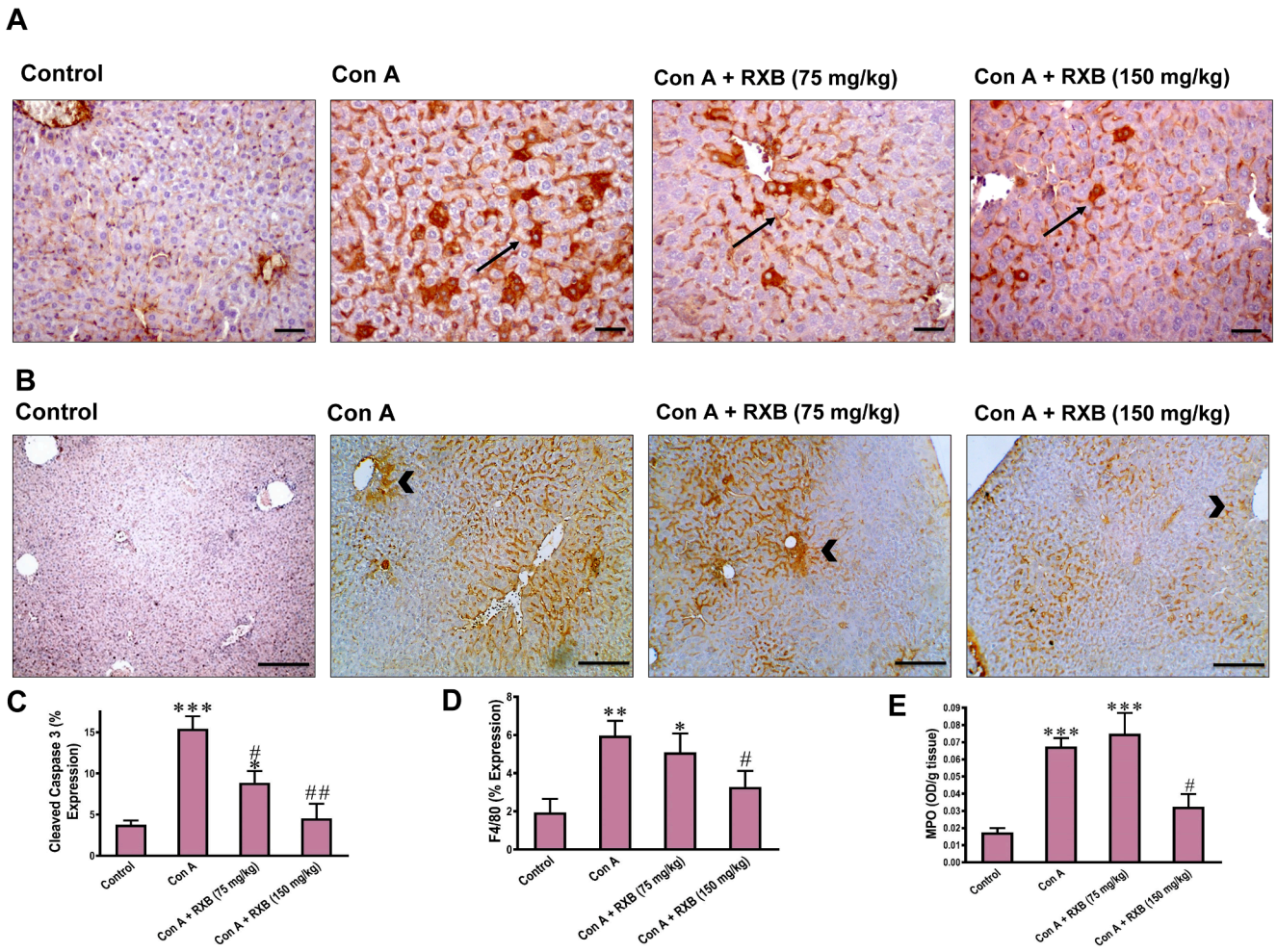

Fig. 4. Impact of RXB pretreatments (75 and 150 mg/kg) for Con A-challenged mice on the immunohistochemical expression and quantification of cleaved caspase 3 (A, C, 400×,), F4/80 (B, D, 100×,) and the activity of MPO (E) in the liver (n = 6–8/group). Arrows indicate apoptotic hepatocytes and arrowheads indicate infiltrated inflammatory cells. *, ** and *** denote a P-value (vs. the Control) less than 0.05, 0.01 and 0.001, respectively, but # and ## denote a P-value (vs. the Con A) less than 0.05 and 0.01, respectively.

3.8. RXB counters lipid peroxidation and nitrosative stress elicited by Con A in the liver

Next, we investigated whether RXB protective effect on Con A-mediated hepatocellular injury was related to oxidative stress. Accordingly, products of lipid peroxidation (MDA and 4-HNE) and nitrosative (NOx) stress were assessed in the liver. Mice intoxicated by Con A alone had a marked ($P < 0.001$) rise of MDA, 4-HNE and NOx concentrations in the liver, compared to the normal control counterparts (Fig. 6E-G). Con A-induced rise of hepatic concentration of MDA was dose-dependently lowered by RXB pretreatments, while those of 4-HNE and NOx were reduced by both doses of RXB pretreatments to the same extent. We also assessed SOD activity in the liver, which was surprisingly increased by Con A alone or with RXB treatments (Fig. 6H).

4. Discussion

Here, we examined the pharmacological inhibition of JAK by RXB prior Con A-challenge. The results demonstrated that JAK inhibition abrogated Con A-induced hepatic injury (ALT, AST, LDH) and necrosis (histopathology). The protection potential of JAK inhibition was further confirmed by lowering Con A-induced apoptosis (cleaved caspase 3) and proliferation as a response of hepatocyte damage (PCNA). Moreover, JAK inhibition abated Con A-induced activation and nuclear transfer of NF-κB in hepatocytes occurring before apoptosis. RXB-pretreatment for Con A-exposed mice was also efficient in reducing the hepatic production and systemic release of the proinflammatory mediators (TNF-α, IFN-γ, IL-17A, IL-1β), as well as decreasing Con A-infiltration of monocytes (F4/80) and neutrophil (MPO).

The major mechanism of hepatic injury elicited by Con A is dependent primarily on TNF-α and IFN-γ [27,28]. Following IV entry of Con A, it binds to mannose-rich glycoproteins on the liver sinusoidal endothelial cells and Kupffer cells. T cells are activated by crosslinking their T cell receptors to these cells and subsequently secrete both IFN-γ and TNF-α that induce apoptotic cell death in liver sinusoidal endothelial cells and hepatocytes, as well as neutrophil recruitment [18]. IFN-γ has also a role like that of TNF-α in Con A-hepatocellular death, because occurrence of hepatitis and Fas-induced apoptosis was decreased significantly in mice lacking IFN-γ [29]. Another pathogenic mechanism happens alongside the first one includes T cell activation for Kupffer cell to secrete TNF-α, ROS and IL-1β-dependent on the assembly of the NLRP3-inflammasome [30]. As a result of this established inflammatory cytokine storm, necrotic and apoptotic cell death of hepatocytes and release of transaminases into the blood circulation occur.

Most proinflammatory cytokines are well-known upon their release to upregulate their self and other cytokines expressions. JAKs were reported to be a downstream for receptors stimulated by IL-6, IFN-γ, TNF-α, IL-1β and others [5]. For instance, binding of IFN-γ to IFN-γ receptors 1/2 triggers activation of JAKs, followed by activation of STAT1/3, NF-κB and transcription of M1 genes in macrophages [31]. Activated M1

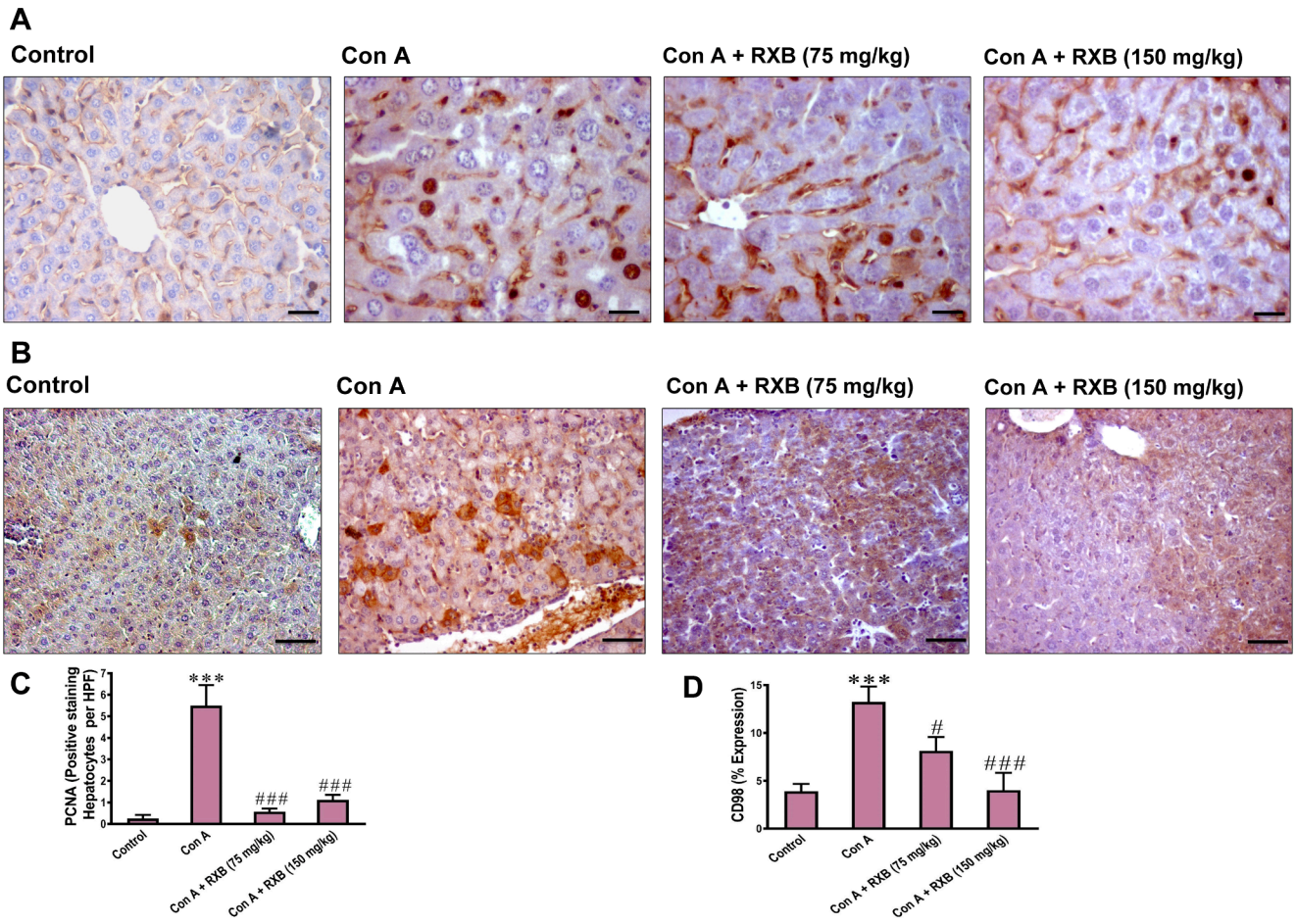

Fig. 5. Impact of RXB pretreatments (75 and 150 mg/kg) for Con A-challenged mice on the hepatic immunohistochemical expression and quantification of PCNA (A and C; 400 ×) and CD98 (B and D; 200 ×) (n = 6–8/group). *** denotes a P-value (vs. the Control) less than 0.001, but # and ### denote a P-value (vs. the Con A) less than 0.05 and 0.001, respectively.

macrophages favor the proinflammatory response *via* increased secretion of chemokines, IL-1β, TNF-α, ROS and RNS, but decreased secretion of IL-10 [32]. TNF-α has been shown to phosphorylate JAKs in several types of immune cells [33,34]. A previous study reported that TNF-α mediated hepatocellular apoptosis through caspase-1, and pretreating con A-exposed mice by tumor necrosis factor-binding protein lessened that apoptosis [35]. Pretreating mice by the IL-1β-receptor antagonist anakinra lowered Con A-induced hepatic damage and phosphorylation of JAK2 and STAT3, as well as IL-17A and ROS generation [30].

Con A was reported to elicit differentiation of Th17 cells producing IL-17A, leading to accrual of TNF-α and IL-6 secretions *via* stimulating dendritic cells, neutrophils and Kupffer cells [36]. The JAK-STAT pathway has an important role in conversion of T helper cells into Th1, Th2, Th17 and regulatory T cells [37]. Moreover, the genetic deletion of STAT3 in T cells reduced Con A-mediated hepatitis and IL-17A production [38]. It has been previously reported that Con A induced inflammation and phosphorylation of STAT3 by activation of JAK2, but these outcomes were blocked by AG490, a selective JAK2 inhibitor [39]. Hence, inhibition of JAK2/STAT3 by RXB limited Con A-induced elevation in hepatic production and systemic release of the proinflammatory IL-17A. Con A also induces regulatory T cells and M2-converted macrophages to secrete IL-10 that is involved in the intrahepatic immune tolerance to limit the overwhelming inflammation [40,41]. While IL-10 receptor signaling is mediated *via* the JAK-STAT pathway [42], RXB-mediated inhibition of this pathway may impair the anti-inflammatory dependent signaling of IL-10. Nevertheless, this interference with IL-10 will not hinder RXB-hepatoprotection against Con A due to dampening the parallel production of the proinflammatory mediators TNF-α, IFN-γ, IL-17A and IL-1β.

Con A-insult led also to hepatic overexpression of CD98, which was lowered by RXB pretreatments in a dose dependent manner. CD98 works as an amino acid transporter by its extracellular domain on hepatocytes, where it is regulates β1-integrin signaling under control of IFN-γ [43,44]. Selective targeting of CD98 markedly reduced the progression and inflammation in non-alcoholic fatty liver disease and lowered even the production of its modulator IFN-γ [44]. Thus, RXB-induced decrease of IFN-γ stimulation lessened the expression of hepatic CD98 that eventually decreased IFN-γ again by feedback.

The link of oxidative stress to Con A-induced hepatitis is not fully known. This can be attributed to Con A-induced overexpression of proinflammatory mediators, leading to enhanced production of ROS and RNS, which aggravated the initial insult mediated by the inflammatory cytokines. The thiol donor N-acetyl cysteine also mitigated the NLRP3-inflammasome assembly and hepatic inflammation caused by Con A, pointing to a key role of GSH in driving the axis of ROS/NLRP3-inflammasome activation [30]. Moreover, Con A directly caused a decline in the cellular GSH content of primary cultured murine hepatocytes [45]. Pretreating the Con A-mice by RXB lowered both RNS and ROS as indicated by MDA, 4-HNE and NOx concentrations in the liver. Our data also showed that these effects were preceded and mediated by restoration of the hepatic GSH and GSH peroxidase. Meanwhile, RXB attenuated Con A-induced rise of SOD, leading to less conversion of superoxide anion radical into hydrogen peroxide. Similarly, Con A-abnormal increase in hepatic GSH reductase and GSH transferase

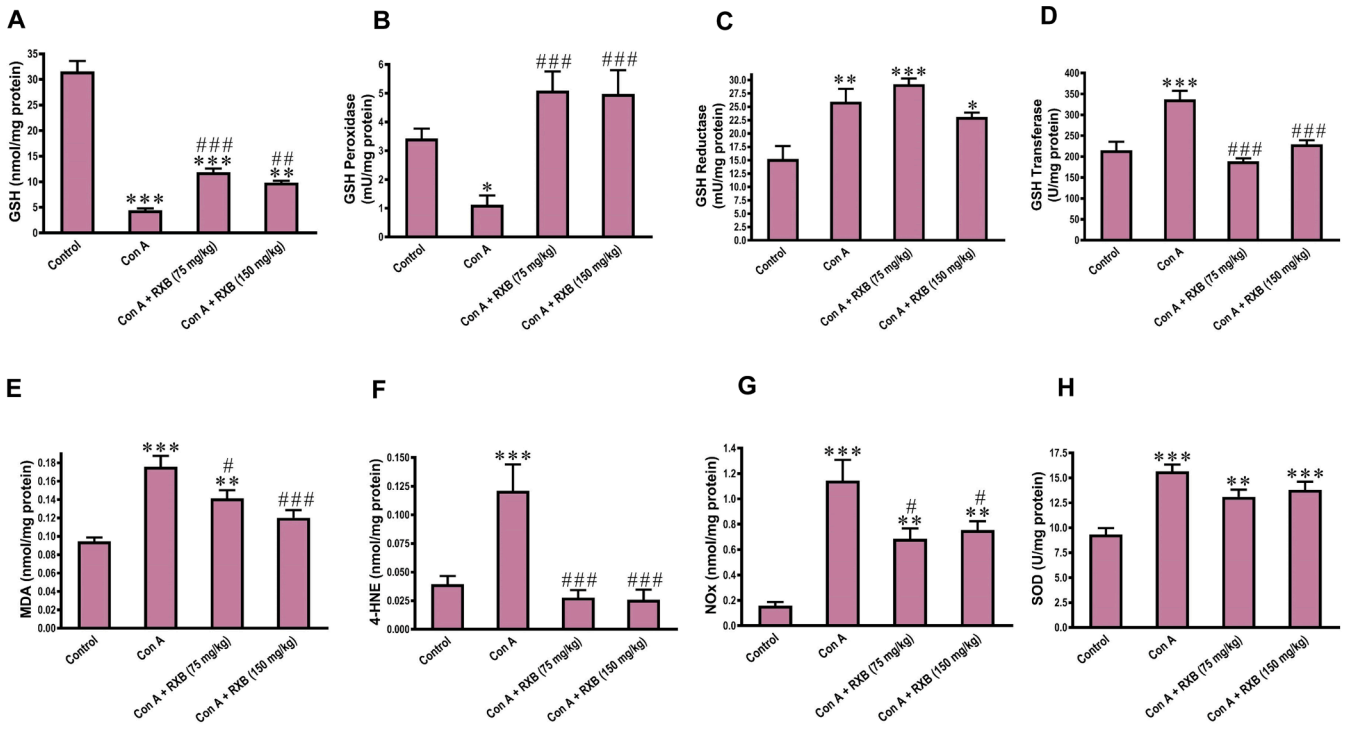

Fig. 6. Impact of RXB pretreatments (75 and 150 mg/kg) for Con A-challenged mice on the hepatic concentrations of GSH (A), GSH peroxidase (B), GSH reductase (C), GSH transferase (D), MDA (E), 4-HNE (F), NOx (G) and SOD (H) (n = 6–8/group). *, ** and *** denote a P-value (vs. the Control) less than 0.05, 0.01 and 0.001, respectively, but #, ## and ### denote a P-value (vs. the Con A) less than 0.05, 0.01 and 0.001, respectively.

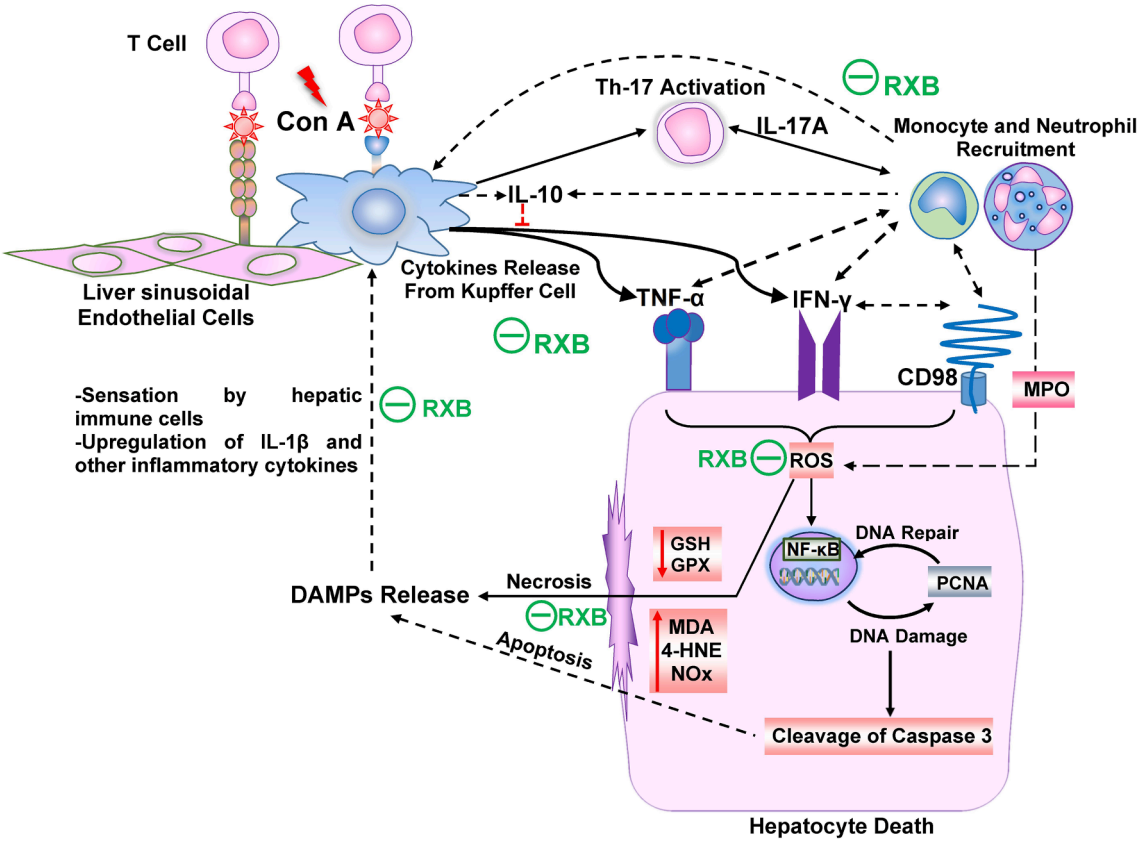

Fig. 7. Schematic illustration of the impact of RXB on Con A-hepatitis.

activities was reduced by RXB, because of decreasing Con A-enhanced depletion of GSH.

In conclusion, pretreatment with RXB spared the liver from the deleterious manifestations of Con A *via* targeting various inflammation cascades, leading to less infiltration of immune cells in the liver (Fig. 7). These comprise mitigating the hepatic overexpression and release of TNF-α, INF-γ and IL-17A alongside the anti-inflammatory IL-10. RXB also lessened the hepatic overexpression of IL-1β and CD98 alongside NF-κB activation, as well as ameliorating the oxidative stress.

Declaration of Competing Interest

The authors declare that they have no known competing financial interests or personal relationships that could have appeared to influence the work reported in this paper.

References

[1] L. Yang, X. Xie, Z. Tu, J. Fu, D. Xu, Y. Zhou, The signal pathways and treatment of cytokine storm in COVID-19, Signal Transduct. Target Ther. 6 (1) (2021) 255.

[2] W. Luo, Y.X. Li, L.J. Jiang, Q. Chen, T. Wang, D.W. Ye, Targeting JAK-STAT Signaling to Control Cytokine Release Syndrome in COVID-19, Trends Pharmacol. Sci. 41 (8) (2020) 531–543.

[3] A. Sharma, P. Jaiswal, Y. Kerakhan, L. Saravanan, Z. Murtaza, A. Zergham, N. S. Honganur, A. Akbar, A. Deol, B. Francis, S. Patel, D. Mehta, R. Jaiswal, J. Singh, U. Patel, P. Malik, Liver disease and outcomes among COVID-19 hospitalized patients - A systematic review and meta-analysis, Ann. Hepatol. 21 (2021), 100273.

[4] J. Wu, S. Song, H.C. Cao, L.J. Li, Liver diseases in COVID-19: Etiology, treatment and prognosis, World J. Gastroenterol. 26 (19) (2020) 2286–2293.

[5] R. Morris, N.J. Kershaw, J.J. Babon, The molecular details of cytokine signaling via the JAK/STAT pathway, Protein Sci. 27 (12) (2018) 1984–2009.

[6] M.C. Freitas, Y. Uchida, D. Zhao, B. Ke, R.W. Busuttil, J.W. Kupiec-Weglinski, Blockade of Janus kinase-2 signaling ameliorates mouse liver damage due to ischemia and reperfusion, Liver Transpl. 16 (5) (2010) 600–610.

[7] S.Y. Shi, C.T. Luk, S.A. Schroer, M.J. Kim, D.W. Dodington, T. Sivasubramaniyam, L. Lin, E.P. Cai, S.Y. Lu, K.U. Wagner, R.P. Bazinet, M. Woo, Janus Kinase 2 (JAK2) Dissociates Hepatosteatosis from Hepatocellular Carcinoma in Mice, J. Biol. Chem. 292 (9) (2017) 3789–3799.

[8] Y.J. Gu, W.Y. Sun, S. Zhang, X.R. Li, W. Wei, Targeted blockade of JAK/STAT3 signaling inhibits proliferation, migration and collagen production as well as inducing the apoptosis of hepatic stellate cells, Int. J. Mol. Med. 38 (3) (2016) 903–911.

[9] A. Kontzias, A. Kotlyar, A. Laurence, P. Changelian, J.J. O'Shea, Jakinibs: a new class of kinase inhibitors in cancer and autoimmune disease, Curr. Opin. Pharmacol. 12 (4) (2012) 464–470.

[10] M. Gadina, M.T. Le, D.M. Schwartz, O. Silvennoinen, S. Nakayamada, K. Yamaoka, J.J. O'Shea, Janus kinases to jakinibs: from basic insights to clinical practice, Rheumatology (Oxford) 58 (Suppl 1) (2019) i4–i16.

[11] D. Przepiorka, L. Luo, S. Subramaniam, J. Qiu, R. Gudi, L.C. Cunningham, L. Nie, R. Leong, L. Ma, C. Sheth, A. Deisseroth, K.B. Goldberg, G.M. Blumenthal, R. Pazdur, FDA Approval Summary: Ruxolitinib for Treatment of Steroid-Refractory Acute Graft-Versus-Host Disease, Oncologist 25 (2) (2020) e328–e334.

[12] J. Mascarenhas, R. Hoffman, Ruxolitinib: the first FDA approved therapy for the treatment of myelofibrosis, Clin. Cancer Res. 18 (11) (2012) 3008–3014.

[13] L.A. Raedler, Jakafi (Ruxolitinib): First FDA-Approved Medication for the Treatment of Patients with Polycythemia Vera, Am. Health Drug Benefits 8 (2015) 75–79.

[14] F. La Rosée, H.C. Bremer, I. Gehrke, A. Kehr, A. Hochhaus, S. Birndt, M. Fellhauer, M. Henkes, B. Kumle, S.G. Russo, P. La Rosée, The Janus kinase 1/2 inhibitor ruxolitinib in COVID-19 with severe systemic hyperinflammation, Leukemia 34 (7) (2020) 1805–1815.

[15] M. Gatti, E. Turrini, E. Raschi, P. Sestili, C. Fimognari, Janus Kinase Inhibitors and Coronavirus Disease (COVID)-19: Rationale, Clinical Evidence and Safety Issues, Pharmaceuticals 14 (8) (2021) 738.

[16] I. Wijaya, R. Andhika, I. Huang, A. Purwiga, K.Y. Budiman, M.H. Bashari, L. Reniarti, R.M.A. Roesli, The use of Janus Kinase inhibitors in hospitalized patients with COVID-19: Systematic review and meta-analysis, Clin. Epidemiol. Glob Health 11 (2021), 100755.

[17] G. Tiegs, J. Hentschel, A. Wendel, A T cell-dependent experimental liver injury in mice inducible by concanavalin A, J. Clin. Invest. 90 (1) (1992) 196–203.

[18] F. Heymann, K. Hamesch, R. Weiskirchen, F. Tacke, The concanavalin A model of acute hepatitis in mice, Lab. Anim. 49 (1 Suppl) (2015) 12–20.

[19] M.M. Bradford, A rapid and sensitive method for the quantitation of microgram quantities of protein utilizing the principle of protein-dye binding, Anal. Biochem. 72 (1976) 248–254.

[20] S. Marklund, G. Marklund, Involvement of the superoxide anion radical in the autoxidation of pyrogallol and a convenient assay for superoxide dismutase, Eur. J. Biochem. 47 (3) (1974) 469–474.

[21] M.E. Shaker, S.A. Ashamallah, M. El-Mesery, The novel c-Met inhibitor capmatinib mitigates diethylnitrosamine acute liver injury in mice, Toxicol. Lett. 261 (2016) 13–25.

[22] M.S. Moron, J.W. Depierre, B. Mannervik, Levels of glutathione, glutathione reductase and glutathione S-transferase activities in rat lung and liver, Biochim. Biophys. Acta 582 (1) (1979) 67–78.

[23] W.H. Habig, M.J. Pabst, W.B. Jakoby, Glutathione S-transferases. The first enzymatic step in mercapturic acid formation, J. Biol. Chem. 249 (22) (1974) 7130–7139.

[24] D. Gerard-Monnier, I. Erdelmeier, K. Regnard, N. Moze-Henry, J.C. Yadan, J. Chaudiere, Reactions of 1-methyl-2-phenylindole with malondialdehyde and 4-hydroxyalkenals. Analytical applications to a colorimetric assay of lipid peroxidation, Chem. Res. Toxicol. 11 (10) (1998) 1176–1183.

[25] K.M. Miranda, M.G. Espey, D.A. Wink, A rapid, simple spectrophotometric method for simultaneous detection of nitrate and nitrite, Nitric Oxide 5 (1) (2001) 62–71.

[26] C. Schierwagen, A.C. Bylund-Fellenius, C. Lundberg, Improved method for quantification of tissue PMN accumulation measured by myeloperoxidase activity, J. Pharmacol. Methods 23 (3) (1990) 179–186.

[27] F. Gantner, M. Leist, A.W. Lohse, P.G. Germann, G. Tiegs, Concanavalin A-induced T-cell-mediated hepatic injury in mice: the role of tumor necrosis factor, Hepatology 21 (1) (1995) 190–198.

[28] H. Mizuhara, M. Uno, N. Seki, M. Yamashita, M. Yamaoka, T. Ogawa, K. Kaneda, T. Fujii, H. Senoh, H. Fujiwara, Critical involvement of interferon gamma in the pathogenesis of T-cell activation-associated hepatitis and regulatory mechanisms of interleukin-6 for the manifestations of hepatitis, Hepatology 23 (6) (1996) 1608–1615.

[29] Y. Tagawa, K. Sekikawa, Y. Iwakura, Suppression of concanavalin A-induced hepatitis in IFN-gamma(-/-) mice, but not in TNF-alpha(-/-) mice: role for IFN-gamma in activating apoptosis of hepatocytes, J. Immunol. 159 (3) (1997) 1418–1428.

[30] J. Luan, X. Zhang, S. Wang, Y. Li, J. Fan, W. Chen, W. Zai, S. Wang, Y. Wang, M. Chen, G. Meng, D. Ju, NOD-Like Receptor Protein 3 Inflammasome-Dependent IL-1β Accelerated ConA-Induced Hepatitis, Front. Immunol. 9 (2018) 758.

[31] S. Arora, K. Dev, B. Agarwal, P. Das, M.A. Syed, Macrophages: Their role, activation and polarization in pulmonary diseases, Immunobiology 223 (4–5) (2018) 383–396.

[32] G. Arango Duque, A. Descoteaux, Macrophage cytokines: involvement in immunity and infectious diseases, Front. Immunol. 5 (2014) 491.

[33] S. Miscia, M. Marchisio, A. Grilli, V. Di Valerio, L. Centurione, G. Sabatino, F. Garaci, G. Zauli, E. Bonvini, A. Di Baldassarre, Tumor necrosis factor alpha (TNF-alpha) activates Jak1/Stat3-Stat5B signaling through TNFR-1 in human B cells, Cell Growth Differ. 13 (1) (2002) 13–18.

[34] A. Yarilina, K. Xu, C. Chan, L.B. Ivashkiv, Regulation of inflammatory responses in tumor necrosis factor-activated and rheumatoid arthritis synovial macrophages by JAK inhibitors, Arthritis Rheum. 64 (12) (2012) 3856–3866.

[35] R. Ksontini, D.B. Colagiovanni, M.D. Josephs, C.K. Edwards 3rd, C.L. Tannahill, C. C. Solorzano, J. Norman, W. Denham, M. Clare-Salzler, S.L. MacKay, L. L. Moldawer, Disparate roles for TNF-alpha and Fas ligand in concanavalin A-induced hepatitis, J. Immunol. 160 (8) (1998) 4082–4089.

[36] S. Yan, L. Wang, N. Liu, Y. Wang, Y. Chu, Critical role of interleukin-17/interleukin-17 receptor axis in mediating Con A-induced hepatitis, Immunol. Cell Biol. 90 (4) (2012) 421–428.

[37] F. Seif, M. Khoshmirsafa, H. Aazami, M. Mohsenzadegan, G. Sedighi, M. Bahar, The role of JAK-STAT signaling pathway and its regulators in the fate of T helper cells, Cell Commun. Signal 15 (1) (2017) 23.

[38] F. Lafdil, H. Wang, O. Park, W. Zhang, Y. Moritoki, S. Yin, X.Y. Fu, M.E. Gershwin, Z.X. Lian, B. Gao, Myeloid STAT3 inhibits T cell-mediated hepatitis by regulating T helper 1 cytokine and interleukin-17 production, Gastroenterology 137 (6) (2009) 2125–2135.

[39] N. Akla, J. Pratt, B. Annabi, Concanavalin-A triggers inflammatory response through JAK/STAT3 signalling and modulates MT1-MMP regulation of COX-2 in mesenchymal stromal cells, Exp. Cell Res. 318 (19) (2012) 2498–2506.

[40] F. Ye, S. Yan, L. Xu, Z. Jiang, N. Liu, S. Xiong, Y. Wang, Y. Chu, Tr1 regulatory T cells induced by ConA pretreatment prevent mice from ConA-induced hepatitis, Immunol. Lett. 122 (2) (2009) 198–207.

[41] Q. Yang, Y. Shi, J. He, Z. Chen, The evolving story of macrophages in acute liver failure, Immunol. Lett. 147 (1–2) (2012) 1–9.

[42] J.K. Riley, K. Takeda, S. Akira, R.D. Schreiber, Interleukin-10 receptor signaling through the JAK-STAT pathway. Requirement for two distinct receptor-derived signals for anti-inflammatory action, J. Biol. Chem. 274 (23) (1999) 16513–16521.

[43] Y. Yan, G. Dalmasso, S. Sitaraman, D. Merlin, Characterization of the human intestinal CD98 promoter and its regulation by interferon-gamma, Am. J. Physiol. Gastrointest. Liver Physiol. 292 (2) (2007) G535–G545.

[44] B.S. Canup, H. Song, V. Le Ngo, X. Meng, T.L. Denning, P. Garg, H. Laroui, CD98 siRNA-loaded nanoparticles decrease hepatic steatosis in mice, Dig. Liver Dis. 49 (2) (2017) 188–196.

[45] M. Leist, A. Wendel, A novel mechanism of murine hepatocyte death inducible by concanavalin A, J. Hepatol. 25 (6) (1996) 948–959.